Anionic and Upper-Excited Fluorescence of C_{60} Encapsulated in Y Zeolitic Nanocavity

Oh-Hoon Kwon,[†] Hyojong Yoo,[†] Kyuchan Park,[†] Bo Tu,[‡] Ryong Ryoo,[§] and Du-Jeon Jang*,[†]

School of Chemistry and Molecular Engineering, Seoul National University, Seoul 151-742, Korea and Department of Chemistry, KAIST, Taejon 305-701, Korea

Received: December 4, 2000; In Final Form: February 14, 2001

C_{60} inserted into a Y zeolitic nanocavity shows anomalous upper-excited fluorescence as well as anionic and normal fluorescence. The intercalation of C_{60} into the supercage of the zeolite has been confirmed by measuring ^{129}Xe NMR spectra while the formation of $^{\bullet}C_{60}^{-}$ has been identified by measuring its ESR spectrum. Time-resolved fluorescence spectra show that the upper-excited fluorescence has the maximum intensity at 450 nm and decays in 28 ps to give birth to the normal fluorescence with the maximum at 750 nm. The normal one decays on the time scale of 1700 ps, while the anionic fluorescence with the maximum intensity at 770 nm has a shorter lifetime of 170 ps.

Introduction

The physical and chemical properties of C_{60} have attracted a great deal of research interest since the success in the preparation of macroscopic quantities of C_{60}.[1−4] There has been much research for the intercalation of C_{60} molecules in the cages and channels of zeolites,[5−13] because the interactions of zeolites with encapsulated chemical species are drastically different from the interactions of solvent molecules with solute species in solutions.[14−16] The incorporation of C_{60} molecules into the robust nanocavities of faujasite zeolites[5−8] would be more interesting than the insertion into the extra large zeolitic pores,[9−13] because there are no physical barriers to immobilize C_{60} into the latter pores. However, the reported electron diffractogram pattern of C_{60}-doped Y zeolite, which is a type of faujasite zeolite, shows that only a small fraction of C_{60} molecules penetrate into nanocavities.[5] Any direct evidence such as ^{129}Xe NMR spectra has not been shown yet on the intercalation of C_{60} into faujasite zeolitic pores. ^{129}Xe NMR spectroscopy has been used as a sensitive tool to confirm the encapsulation of organic molecules in zeolitic nanocavities.[17,18]

The absorption spectra of C_{60} in solutions reveal a strong absorption between 200 and 400 nm, and a very weak broad absorption in the 400−700 nm region.[3] The very weak absorption in the visible region is due to first-order-forbidden transitions. As the fullerene molecules form charge-transfer complexes with electron donating molecules, the intensity of the symmetry-forbidden lowest absorption band is reported to increase.[19] A strong absorption band at 1064 nm, absent in the C_{60} spectrum, has been attributed to the allowed electric-dipolar transition of $^{\bullet}C_{60}^{-}$.[20] ESR spectroscopy has been employed to investigate the formation of $^{\bullet}C_{60}^{-}$ in various circumstances.[21,22] C_{60} in solutions is reported to show a broad fluorescence band between 650 and 850 nm.[23,24] Very recently, the fine particles of C_{60} in ethanol are reported[4] to show fluorescence with the peak around 730 nm, which is similar to that of C_{60} in benzene solution. The lifetime of C_{60} has been reported to be 0.65[25] or 1.2 ns[26,27] in neutral solvent and 1.2 ns[28−31] in film. The C_{60} incorporated in VPI-5 zeolite is reported to have the decay time of 1.2 ns.[9]

We report here that ^{129}Xe NMR spectra have been measured for the first time to confirm the successful intercalation of C_{60} molecules into Y zeolitic nanocavities. The formation of $^{\bullet}C_{60}^{-}$ is confirmed as well by measuring ESR spectra. The C_{60} encapsulated in the Y zeolitic nanocavity shows anomalous upper-excited fluorescence as well as anionic and normal fluorescence. We have measured the time-resolved spectra as well as the lifetimes for the individual fluorescence bands.

Experimental Section

Materials. C_{60}, purchased from Sigma, was used without further purification. Na^{+}-exchanged Y zeolite (NaY) of high purity was synthesized, washed with doubly distilled hot water, and dried in a vacuum oven. After dehydration at 400 °C for 5 h and cooling to room temperature, the typical unit cell formula of NaY was found to be $Na_{56}(AlO_2)_{56}(SiO_2)_{136}\cdot 250H_2O$. Dehydrated NaY zeolite with 1.0 mmol of the supercage was mixed with 25 μmol of C_{60} in a quartz tube. The tube was evacuated, sealed, and maintained at 650 °C for 72 h in order to make C_{60} sublime and diffuse uniformly into zeolite supercages. Then it was cooled slowly to room temperature. X-ray diffraction was used to confirm that the framework structures of C_{60}-introduced NaY (C_{60}Y) did not change during the dehydration and intercalation processes.

Static Measurements. ^{129}Xe gas (Matheson, 99.995%) was equilibrated with a sample contained in an NMR tube through a stopcock before a ^{129}Xe NMR spectrum was measured using an NMR spectrometer (Bruker, AM-300). ESR derivative curves were measured at the X band using an ESR spectrometer (Bruker, ESP 300). Fluorescence spectra were obtained using a home-built fluorometer, which consisted of a 75 W Xe lamp (Acton Research, XS 432), 0.15 m and 0.30 m monochromators (Acton Research, Spectrapro 150 and 300), and a photomultiplier tube (Acton Research, PD438).

Time-Resolved Fluorescence Measurements. Pulses (355 or 532 nm) of 25 ps duration from an actively and passively mode-locked Nd:YAG laser (Quantel, YG 701) were employed

* To whom correspondence should be addressed. Telephone: +82-2-875-6624. Fax: +82-2-889-1568. E-mail: djjang@plaza.snu.ac.kr.
† Seoul National University.
‡ Present address: Department of Chemistry, Fudan University, Shanghai 200433, China.
§ KAIST.

10.1021/jp0043625 CCC: $20.00
Published on Web 04/12/2001

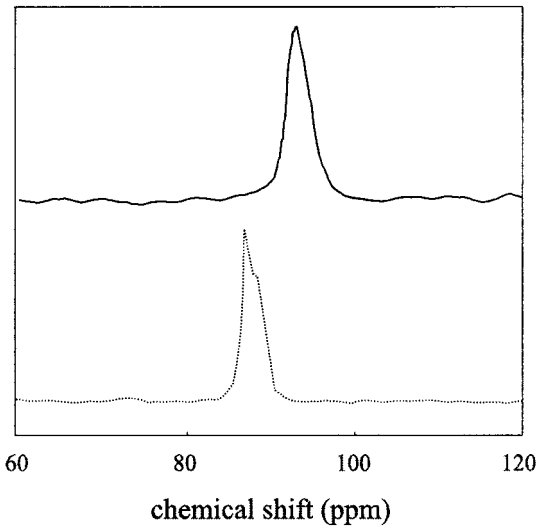

Figure 1. ^{129}Xe NMR spectra of $C_{60}Y$ (solid) and NaY (dotted), which show the chemical shifts of 93 and 87 ppm, respectively.

to excite samples. The fluorescence wavelength was selected using a 0.15 m monochromator (Acton Research, Spectrapro 150) and combined band-pass filters for time-resolved spectra and kinetic profiles, respectively. Fluorescence kinetic curves were detected using a 10 ps streak camera (Hamamatsu, C2830), attached with a CCD (Princeton Instruments, RTE-128-H). Time-resolved fluorescence spectra were corrected against the wavelength-dependent variation of detector sensitivity. Fluorescence kinetic constants were extracted by fitting a measured kinetic profile to a computer-simulated kinetic curve convoluted with the temporal response function iteratively.

Results and Discussion

The ^{129}Xe NMR chemical shift of $C_{60}Y$ is larger by 6 ppm than that of NaY (Figure 1). The larger shift is due to the strong interactions of Xe atoms with organic C_{60} molecules in addition to collisions with the supercage wall and other xenon atoms present in bare NaY. The observation of a single peak at a new position indicates that C_{60} is inserted into the supercage of NaY uniformly from a macroscopic viewpoint. The chemical shift arises from the collisions of xenon atoms with the C_{60} molecules in the supercages, with the walls of the supercages, and with the xenon atoms, as they move about zeolite particles. While the Xe atoms experience numerous collisions at totally different sites, a single Lorentzian NMR peak reflects only an average environment on the time scale of the NMR measurement, weighted by the respective collision probabilities.[32,33] Considered that only the 0.025 fraction of the supercages contain C_{60} molecules, the interaction between C_{60} and Xe gives birth to a very large chemical shift. Many attempts have been made at various temperatures to intercalate C_{60} into the supercage with keeping the structural integrity, until the optimum temperature is determined as ~650 °C. This is about the lowest temperature where C_{60} can be inserted satisfactorily into the zeolitic nanocavity in a vacuum without affecting the crystalline structure.

We are reporting ^{129}Xe NMR spectra for the first time to our knowledge to confirm the intercalation of C_{60} into faujasite zeolitic nanocavities, although the intercalation have been reported in various zeolites.[5−13] Taking into account that C_{60} is a spherical molecule with a diameter of 0.70 nm, we have chosen NaY as the matrix to take advantage of three-dimensional supercage pores. The supercages are nanocavities having the diameter of 1.3 nm and they are tetrahedrally connected through 0.74 nm channels. The chemical shift of adsorbed xenon is reported[33−35] to increase only if organic molecules are adsorbed inside zeolitic pores. Our additional chemical shift of 6 ppm with the introduction of 0.025 C_{60} molecule per supercage indicates that C_{60} molecules are really intercalated into zeolitic nanocavities.

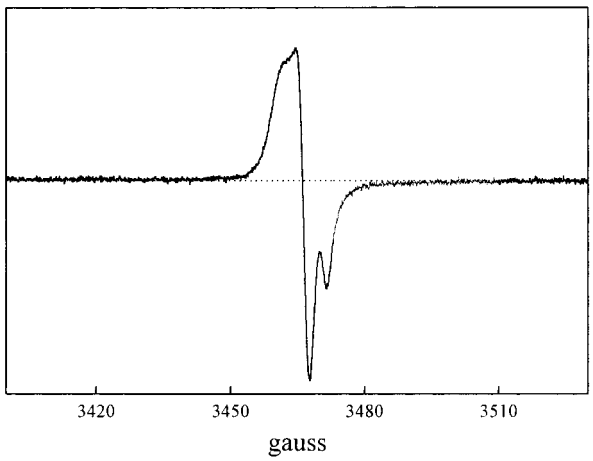

Figure 2. ESR spectrum of $C_{60}Y$, showing the *g*-factor of 2.0058.

The ESR spectrum in Figure 2 indicates that the C_{60} adsorbed at the wall surface of the supercage forms an anionic radical species of $^{\bullet}C_{60}^{-}$ and that the radical anion is stable enough to exist at the ground state in the nanocavity of NaY. While bare NaY yields a very weak broad ESR spectrum, $C_{60}Y$ brings in a new intense sharp spectrum with a *g*-value of 2.0058, which is a typical value for organic radicals. Our ESR spectrum is very different from reported ones for solutions[21,22,36] in two aspects. Its *g*-value is significantly larger than those (2.0006,[21] 1.998,[22] 2.001[36]) in solutions, and the spectrum is too multiplex to originate from a single species of $^{\bullet}C_{60}^{-}$ in a same environment. The *g*-value of 2.0022 for HC_{60} in solution[37] is reported to be much larger than that for $^{\bullet}C_{60}^{-}$ in solution.[21,22,36] Our ESR spectrum looks like the signal of free organic radicals superimposed with the signals of polarized organic radicals split into multiplets by neighboring nuclear spins. Considering these, we suggest temporarily that the radical anions are formed in zeolitic nanocavities and that they exist in different environments. Some of $^{\bullet}C_{60}^{-}$ have protons or sodium ion clusters nearby. Protons are available to form the protonated species of $^{\bullet}C_{60}^{-}$ ($H^{+}C_{60}^{-}$),[37] as a dehydrated sample still contains a great number of hydrated water molecules.[38] The large *g*-value, compared with those of $^{\bullet}C_{60}^{-}$ and $H^{+}C_{60}^{-}$ in solution,[36,37] is due to the polar environment of the radical anion, and the multiplex structure is attributed to the heterogeneous environment in the nanocavity surface. We consider that the reported small *g*-values in faujasite zeolites[6−8] are due to the anions located at the external surface rather than inside the nanocavity.

Many research groups have reported on the fluorescence of C_{60} in solutions[25,26] or in solid films.[28−31] As reported in other zeolites,[7−11] the static luminescence spectrum of $C_{60}Y$ given in Figure 3 is shifted to the blue very significantly compared with the luminescence spectra of C_{60}-dissolved solutions.[4,19] The spectrum of $C_{60}Y$ is also spectrally broader than the latter ones. With excitation at 355 nm the luminescence of $C_{60}Y$ shows the maximum intensity at 600 nm and it shifts to the red by 15 nm with excitation at 532 nm. Absorption resulting from the first-order-forbidden transition between the h_u and t_{1u} configurations enhances for C_{60} intercalated in the supercage of zeolite, since the symmetry of the C_{60} is distorted due to the interaction with

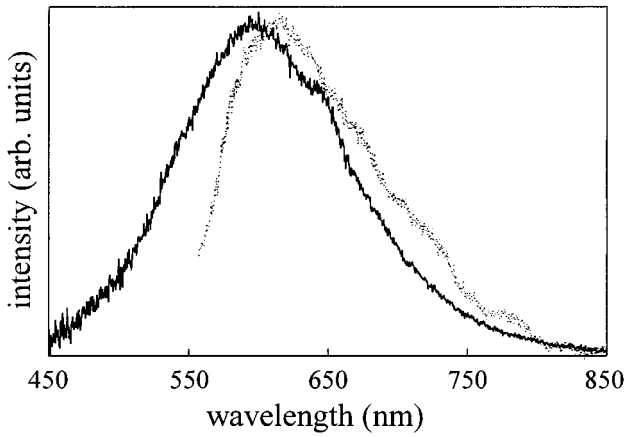

Figure 3. Background-subtracted emission spectra of $C_{60}Y$ with excitation at 355 (solid) and 532 nm (dotted). The solid and dotted spectra show their maxima at 600 and 615 nm, respectively. Although background luminescence has been subtracted, it is still contained in both shown spectra considerably. This is because the raw intensity of background luminescence is larger than that of C_{60} luminescence and both intensities are not distinguishable in static emission spectra.

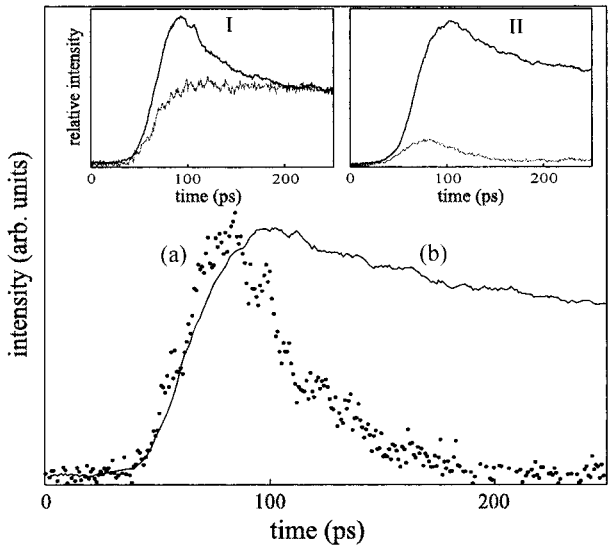

Figure 4. Background-free fluorescence kinetic profiles, excited at 355 nm (a, b) and monitored at 435 ± 30 nm (a) and 660+ nm (b), of C_{60} intercalated in the supercage of NaY. Insets: observed raw emission kinetic profiles, monitored at 435 ± 30 nm (I) and 660+ nm (II), of $C_{60}Y$ (solid) and NaY (dotted).

the zeolitic surface. In particular, $^{\bullet}C_{60}^{-}$ would experience a stronger enhancement in the absorption than C_{60} because the anions interact strongly with protons, sodium ions, or cation clusters at the surface of the zeolitic nanocavities. Thus, the red shift in the luminescence spectrum of $C_{60}Y$ with excitation at 532 nm is due to a relative decrease in the upper-excited fluorescence of C_{60} and a relative increase in the anionic fluorescence of $^{\bullet}C_{60}^{-}$ (vide infra). Although the upper-excited fluorescence, as well as the anionic fluorescence and the different environment, contributes to make $C_{60}Y$ luminescence spectrally different from the fluorescence of C_{60} in solutions, the main reason for the spectral difference is found to be that the background luminescence present in C_{60}-free bare NaY interferes strongly with C_{60} or $^{\bullet}C_{60}^{-}$ fluorescence.

By measuring the background-free fluorescence kinetic profiles (Figures 4 and 5) and time-resolved spectra (Figure 6) of C_{60} in NaY nanocavities, we have determined not only the individual lifetimes but also spectra of the upper-excited, normal, and anionic fluorescence bands for C_{60} intercalated in the zeolitic

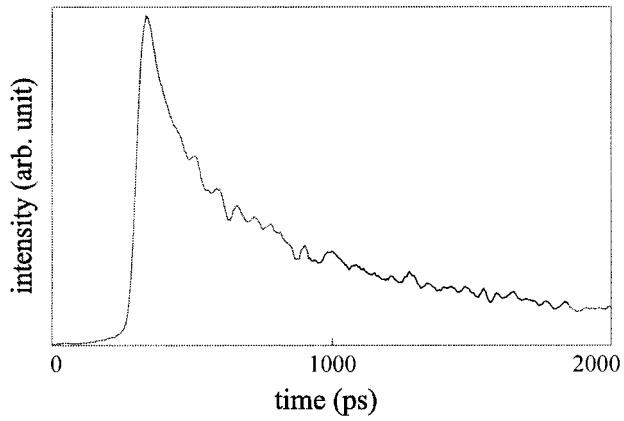

Figure 5. Background-free fluorescence kinetic profiles, excited at 355 nm and monitored at 660+ nm, of C_{60} introduced in NaY in a long time window.

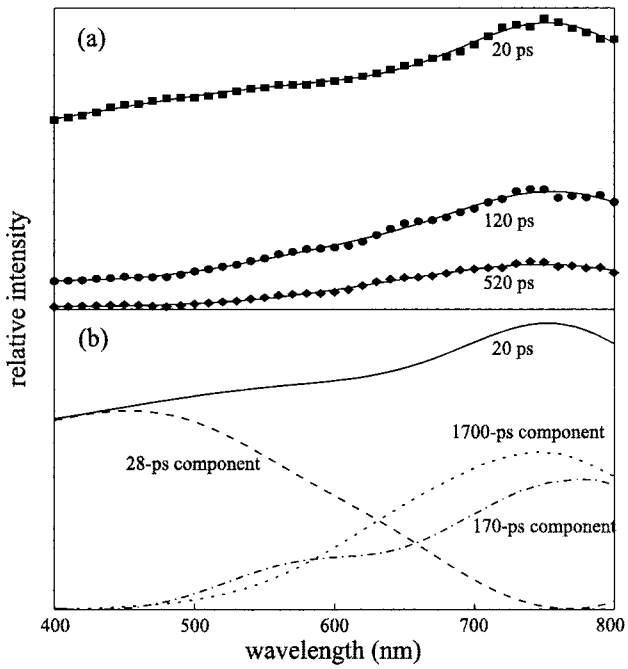

Figure 6. Background-free time-resolved fluorescence spectra, at the given delay times after excitation, of C_{60} encapsulated in the supercage of NaY (a) and deconvoluted relative contributions of individual components to the fluorescence spectrum at 20 ps delay (b). Solid curves are computer-smoothened time-resolved spectra at given delay times.

nanocavity of NaY. To our knowledge, we are reporting the upper-excited fluorescence spectrum of C_{60} for the first time. Considering that static emission intensity is proportional to the lifetime as well as the initial amplitude, inset I in Figure 4 indicates that the directly observed raw static luminescence spectra of C_{60}-introduced zeolites are dominated by C_{60}-independent background luminescence rather than by C_{60} fluorescence. Emission kinetic profiles allow us to separate C_{60} fluorescence from background luminescence because two contributions behave in extremely different time scales.

The fluorescence of C_{60} in the zeolitic nanocavity decays faster in the blue region than in the red region. As shown with the fluorescence kinetic time constants (Table 1), extracted from the background-free kinetic profiles in Figures 4 and 5, with our current experimental method we can distinguish three fluorescence components that have extremely different lifetimes. The blue fluorescence decays in 28 ps to bring in the red fluorescence that decays on the time scale of 1700 ps. Besides

TABLE 1: Fluorescence Kinetic Constants Deconvoluted from the Profiles in Figures 4 and 5

figure	λ_{em} (nm)	window time (ps)	fluorescence time constant (ps)	
			rise	decay
4	435 ± 30	250	instant	28
4	660+	250	instant (52%)[a] + 28	170 (52%) + 1700
5	660+	2000	instant	170 (74%) + 1700

[a] Intensity percentage of each component.

the slow decaying component, there is another red component that decays on the time scale of 170 ps. The blue component is ascribed to upper-excited fluorescence emitted from the upper-excited $^1t_{1g}$ configuration of the neutral C_{60} species. The red component rising in 28 ps and decaying in 1700 ps is assigned to normal fluorescence emitted from the lowest-excited $^1t_{1u}$ configuration of C_{60}. On the other hand, the red component rising instantly and decaying in 170 ps is due to anionic fluorescence from the $^2t_{1u}$ configuration of $^\bullet C_{60}^-$. Because of the anionic fluorescence rising instantly, the apparent rise of the red fluorescence is faster than the decay of the blue fluorescence. Nevertheless, the relatively slow rise of the red fluorescence and the agreement among the kinetic constants in Table 1, together with the time-resolved fluorescence spectra in Figure 6, have led us to assign the respective emitting states of the three decay components confidently. Furthermore, the decay times of the normal and anionic fluorescence bands have been resolved unambiguously because they are different as extensively as by a factor of 10.

As expected from Figures 4 and 5, a static luminescence spectrum of C_{60}-contained NaY is dominated by the background luminescence. Thus, we have measured time-resolved emission spectra by subtracting background luminescence to get the individual spectral features of the three components. The time-resolved emission spectra of Figure 6a obviously show that the emission decays faster in the blue than in the red, as discussed already. However, the time-resolved spectra are too featureless to reveal the individual spectra of the three components directly. If fluorescence intensity is measured at three different delay times, it can be divided into the three components at every measured wavelength. Fluorescence intensity at a certain wavelength and at a given time t in the unit of picoseconds, $I(t)$, is the intensity sum of all the components involved as

$$I(t) = f_u \exp(-t/28) + f_a \exp(-t/170) + f_n[1 - \exp(-t/28)] \exp(-t/1700) \quad (1)$$

in which f_u and f_a are the initial intensities of the upper-excited and anionic fluorescence, respectively. The f_n is the theoretical intensity of the normal fluorescence that has risen completely without decaying at all. The respective spectra of the three components in Table 1 can be obtained by linearly combining the time-resolved spectra of Figure 6a according to eq 1.

The upper-excited fluorescence of the 28 ps decay has the maximum intensity near 450 nm, while the normal fluorescence of the 1700 ps decay has the maximum at 750 nm (Figure 6b). On the other hand, the anionic fluorescence of the 170 ps decay has its maximum intensity at 770 nm. At the delay time of 20 ps the intensity of the anionic fluorescence is about comparable with that of the normal fluorescence. Considering ESR signals and static absorbances, we estimate that only a small fraction of C_{60} molecules transform into the anions. The transition between the t_{1u} and h_u configurations is forbidden mainly because the fullerene has a center of inversion. As C_{60} is adsorbed at the zeolitic surface, the selection rule becomes less strict. The transition becomes more significant for $^\bullet C_{60}^-$, because the anionic species interacts strongly with cations located in the surface. Even in solutions, the forbidden transition is reported to be stronger for $^\bullet C_{60}^-$ than for C_{60}.[20] Nevertheless, adsorption at the surface of the zeolitic nanocavity enhances the oscillator strength of the t_{1u} emission significantly for $^\bullet C_{60}^-$ as well as for C_{60}. The shoulder of the anionic emission at ~570 nm is suggested to result from the sodium cation clusters[15,39] of $(Na)_n^{n-1+}$ that interact with $^\bullet C_{60}^-$. This again agrees with the multiplex ESR signal and supports our suggestion that $^\bullet C_{60}^-$ interacts strongly with cations in the zeolitic surface of the nanocavity.

The C_{60} molecules trapped in the zeolitic nanocavities of NaY, which has been dehydrated at 400 °C in a vacuum, show extremely different behaviors from those in solutions or in the gas phase. Some of them located at base catalytic sites transform into radical anions. The detailed formation mechanism of the anions will be discussed in a later report. The large g-value and multiplex feature of the ESR spectrum already have been ascribed to the ionic and heterogeneous surroundings of $^\bullet C_{60}^-$ in the cavities. The relaxation of C_{60} excitation energy is slowed in the nanocavity. The relaxation from upper-excited states was reported[40,41] to occur within a few picoseconds. However, the internal conversion from the upper-excited $^1t_{1g}$ to the first-excited $^1t_{1u}$ takes as long as 28 ps in the zeolitic nanocavity. The normal fluorescence lifetime of 1700 ps is also larger than the reported C_{60} fluorescence lifetimes in other circumstances.[9,25-31] We attribute the slow relaxation mainly to the collision-free environment of C_{60} in the cavity. The lifetime of the anionic fluorescence is much shorter than that of the normal one. Neither the static spectrum nor lifetime of the anionic fluorescence emitted from the $^2t_{1u}$ (HOMO) to the ^2h_u (HOMO-1) has been reported yet to our knowledge, although the static spectrum of the anionic fluorescence emitted from the $^2t_{1g}$ (HOMO+1) to the $^2t_{1u}$ is reported in a solution.[42] No report on the anionic fluorescence lifetime probably comes from the fast relaxation of the anionic species. Thus, the observation of 170 ps for the anionic fluorescence lifetime also results from the relaxation-slow effect of the nanocavity. Nonetheless, the relaxation of the anionic species is much faster than that of the neutral species. We suggest that the interaction of two electrons above the h_u facilitates the relaxation of $^\bullet C_{60}^-$ excitation energy. Another effect of the nanocavity is the 20 nm red shift of the normal fluorescence, which is reported to have the maximum at 730 nm in solution.[4] The highly polar environment of the nanocavity surface shifts the (π,π*) transition of C_{60} to the red significantly. It is interesting to note that for the same transition of $t_{1u} \rightarrow h_u$ the anionic fluorescence experiences an additional red shift by 20 nm compared with the normal fluorescence. This is due to the strong interaction of $^\bullet C_{60}^-$ with cations in the zeolitic surface, together with the interaction of two electrons above the h_u configuration. Adsorption at a polar surface and strong interactions with cations significantly enhance the oscillator strength of the symmetry-forbidden emission from the t_{1u} as well. Indeed, the zeolitic nanocavity changes various characters of the very inert species of C_{60} very significantly.

Conclusions

Anomalous upper-excited fluorescence as well as anionic and normal fluorescence is observable from C_{60} encapsulated in a Y zeolitic nanocavity at room temperature. C_{60} can be introduced into the supercage of NaY at 650 °C without affecting the crystalline structure. The radical anions of $^\bullet C_{60}^-$ are present at the ground state in zeolitic nanocavities. The multiplex structure

of the ESR band having a large *g*-value is due to the heterogeneous and polar environment of the anion adsorbed at the nanocavity surface. The upper-excited fluorescence has the maximum intensity at 450 nm and it decays in 28 ps to give birth to the normal fluorescence having the maximum intensity at 750 nm. The normal fluorescence decays in the time scale of 1700 ps. The long lifetimes of the upper-excited and normal fluorescence bands are attributed to the collision-free environment of C_{60} isolated in the supercage. The anionic fluorescence with a decay time of 170 ps has the maximum intensity at 770 nm.

Acknowledgment. The Center for Molecular Catalysis supported this work. D.J.J. and O.H.K. also acknowledge the Korea Research Foundation (KRF-2000-015-DP0193) and the Brain Korea 21 Program, respectively. We thank the Equipment Joint Use Program of the Korea Basic Science Institute as well.

References and Notes

(1) Kroto, H. W.; Heath, J. R.; O'Brien, S. C.; Curl, R. F.; Smalley, R. E. *Nature* **1985**, *318*, 162.

(2) Krätschmer, W.; Lamb, L. D.; Fostiropoulos, K.; Huffman, D. R. *Nature* **1990**, *347*, 354.

(3) Hare, J. P.; Kroto, H. W.; Taylor, R. *Chem. Phys. Lett.* **1991**, *177*, 394.

(4) Fujitsuka, M.; Kasai, H.; Masuhara, A.; Okada, S.; Oikawa, H.; Nakanishi, H.; Ito, O.; Yase, K. *J. Photochem. Photobiol. A: Chem.* **2000**, *133*, 45.

(5) Sastre, G.; Cano, M. L.; Corma, A.; García, H.; Nicolopoulos, S.; González-Calbert, J. M.; Vallet-Regí, M. *J. Phys. Chem. B* **1997**, *101*, 10184.

(6) Keizer, P. N.; Morton, J. R.; Preston, K. F.; Sugden, A. K. *J. Phys. Chem.* **1991**, *95*, 7117.

(7) Gu, G.; Ding, W.; Cheng, G.; Zang, W.; Zen, H.; Zhang, J.; Du, Y. *Mod. Phys. Lett.* **1995**, *9*, 1327.

(8) Gu, G.; Ding, W.; Cheng, G.; Zang, W.; Zen, H.; Du, Y. *Appl. Phys. Lett.* **1995**, *67*, 326.

(9) Lamrabte, A.; Janot, J.-M.; Elmidaoui, A.; Seta, P.; de Ménorval, L.-C.; Backov, R.; Rozière, J.; Sauvajol, J.-L.; Allègre, J. *Chem. Phys. Lett.* **1998**, *295*, 257.

(10) Gu, G.; Ding, W.; Du, Y.; Huang, H.; Yang, S. *Appl. Phys. Lett.* **1997**, *70*, 2619.

(11) Govindaraj, A.; Nath, M.; Eswaramoorthy, M. *Chem. Phys. Lett.* **2000**, *317*, 35.

(12) Gugel, A.; Mullen, K.; Reichert, H.; Schmidt, W.; Schon, G.; Schuth, F.; Spickermann, J.; Titman, J.; Unger, K. *Angew. Chem., Int. Ed. Engl.* **1993**, *32*, 556.

(13) Anderson, M. W.; Shi, J. M.; Leigh, D. A.; Moody, A. E.; Wade, F. A.; Hamilton, B.; Carr, S. W. *J. Chem. Soc., Chem. Commun.* **1993**, 533.

(14) Cizmeciyan, D.; Sonnichsen, L. B.; Garcia-Garibay, M. A. *J. Am. Chem. Soc.* **1997**, *119*, 184.

(15) Park, J.; Kang, W.-K.; Ryoo, R.; Jung, K.-H.; Jang, D.-J. *J. Photochem. Photobiol. A: Chem.* **1994**, *80*, 333.

(16) Ramamurthy, V. *J. Am. Chem. Soc.* **1994**, *116*, 1345.

(17) Ito, T.; Fraissard, J. *J. Chem. Phys.* **1982**, *76*, 5225.

(18) Kang, W.-K.; Cho, S.-J.; Lee, M.; Kim, D.-H.; Ryoo, R.; Jung, K.-H.; Jang, D.-J. *Bull. Korean Chem. Soc.* **1992**, *13*, 140.

(19) Wang, Y. *J. Phys. Chem.* **1992**, *96*, 764.

(20) Greaney, M. A.; Gorun, S. M. *J. Phys. Chem.* **1991**, *95*, 7142.

(21) Kukolich, S. G.; Huffman, D. R. *Chem. Phys. Lett.* **1991**, *182*, 263.

(22) Dubois, D.; Jones, M. T.; Kadish, K. M. *J. Am. Chem. Soc.* **1992**, *114*, 6446.

(23) Kim, D.; Lee, M.; Suh, Y. D.; Kim, S. K. *J. Am. Chem. Soc.* **1992**, *114*, 4429.

(24) Ma, B.; Sun, Y. P. *J. Chem. Soc., Perkin Trans. 2* **1996**, 2157.

(25) Sension, R. J.; Phillips, C. M.; Szarka, A. Z.; Romanow, W. J.; McGhie. A. R.; McCauley, J. P., Jr.; Smith, A. B., III; Hochstrasser, R. M. *J. Phys. Chem.* **1991**, *95*, 6075.

(26) Ebbesen, T. W.; Tanigaki, K.; Kuroshima, S. *Chem. Phys. Lett.* **1991**, *181*, 501.

(27) Yang, L.; Dorsinville, R. *Opt. Commun.* **1996**, *124*, 45.

(28) Byrne, H. J.; Maser, W.; Ruhle, W. W.; Mittelbach, A.; Honle, W.; von Schnering, H. G.; Movaghar, B.; Roth, S. *Chem. Phys. Lett.* **1993**, *204*, 461.

(29) Itaya, A.; Suzuki, I.; Tsuboi, Y.; Miyasaka, H. *J. Phys. Chem. B* **1997**, *101*, 5118.

(30) Sauvé, G.; Dimitrijevic, N. M.; Kamat, P. V. *J. Phys. Chem.* **1995**, *99*, 1199.

(31) Gevaert, M.; Kamat, P. V. *J. Phys. Chem.* **1992**, *96*, 9883.

(32) Boddenberg, B.; Hartmann, M. *Chem. Phys. Lett.* **1993**, *203*, 243.

(33) Chmelka, B. F.; Pearson, J. G.; Liu, S. B.; Ryoo, R.; de Menorval, L. C.; Pines, A. *J. Phys. Chem.* **1991**, *95*, 303.

(34) Ryoo, R.; Liu, S.-B.; de Menorval, L. C.; Takegoshi, K.; Chmelka, B.; Trecoske, M.; Pines, A. *J. Phys. Chem.* **1987**, *91*, 6575.

(35) de Menorval, L. C.; Raftery, D.; Liu, S.-B.; Takegoshi, K.; Ryoo, R.; Pines, A. *J. Phys. Chem.* **1990**, *94*, 27.

(36) Dubois, D.; Kadish, K. M.; Flanagan, S.; Haufler, R. E.; Chibante, L. P. F.; Wilson, L. J. *J. Am. Chem. Soc.* **1991**, *113*, 4364.

(37) Klemt, R.; Roduner, E.; Fischer, H. *Chem. Phys. Lett.* **1994**, *229*, 524.

(38) Lee, S.; Hwang, H.; Kim, P.; Jang, D.-J. *Catal. Lett.* **1999**, *57*, 221.

(39) Iu, K.-K.; Thomas, J. K. *J. Phys. Chem.* **1991**, *95*, 506.

(40) Jacquemin, R.; Kraus, S.; Eberhardt, W. *Solid State Commun.* **1998**, *105*, 449.

(41) Thomas, T. N.; Taylor, R. A.; Ryan, J. F.; Mihailovic, D.; Zamboni, R. *Europhys. Lett.* **1994**, *25*, 403.

(42) Kato, T.; Kodama, T.; Shida, T. *Chem. Phys. Lett.* **1993**, *205*, 405.